

Non-planar coil winding angle optimization for compatibility with non-insulated high-temperature superconducting magnets

C. Paz-Soldan  

General Atomics, PO Box 85608, San Diego, CA 92186-5608, USA

(Received 25 June 2020; revised 1 September 2020; accepted 2 September 2020)

The rapidly emerging technology of high-temperature superconductors (HTS) opens new opportunities for the development of non-planar non-insulated HTS magnets. This type of HTS magnet offers attractive features via its simplicity and robustness, and is well suited for modest size steady-state applications such as a mid-scale stellarator. In non-planar coil applications the HTS tape may be subject to severe hard-way bending strain (ϵ_{bend}), torsional strains (ϵ_{tor}) and magnetic field components transverse to the HTS tape plane (B_{\perp}), all of which can limit the magnet operating space. A novel method of winding angle optimization is here presented to overcome these limitations for fixed input non-planar coil filamentary geometry. Essentially, this method: (i) calculates the peak ϵ_{bend} and B_{\perp} for arbitrary winding angle along an input coil filamentary trajectory, (ii) defines a cost function including both and then (iii) uses tensioned splines to define a winding angle that reduces ϵ_{tor} and optimizes the ϵ_{bend} and B_{\perp} cost function. As strain limits are present even without B_{\perp} , this optimization is able to provide an assessment of the minimum buildable size of an arbitrary non-planar non-insulating HTS coil. This optimization finds that for standard 4 mm wide HTS tapes the minimum size coils of the existing HSX, NCSX and W7-X stellarator geometries are around 0.3–0.5 m in mean coil radius. Identifying the minimum size provides a path to specify a mid-scale stellarator capable of achieving high-field or high-temperature operation with minimal HTS tape length. For coils larger than this size, strain optimization allows use of wider (higher current capacity) HTS tapes or alternatively permitting a finite (yet tolerable) strain allows reduction of B_{\perp} . Reduced B_{\perp} enables a reduction of the HTS tape length required to achieve a given design magnetic field or equivalently an increase in the achievable magnetic field for fixed HTS tape length. The distinct considerations for optimizing a stellarator coilset to further ease compatibility with non-insulated HTS magnets are also discussed, highlighting relaxed curvature limits and the introduction of limits to the allowable torsion.

Key words: fusion plasma, plasma devices

1. Introduction and motivation

High-temperature superconductors (HTS) have been recognized for the past two decades as offering attractive new pathways for magnet development (Bruzzone,

† Email address for correspondence: paz-soldan@fusion.gat.com

Fietz & Minervini 2018). Compared to low-temperature superconductors (LTS), HTS enable the design of magnets that operate at higher magnetic field, higher temperature, higher current density, or combinations of all three. Compared to copper, HTS (and LTS) offer the benefit of significantly reduced energy dissipation within the magnet, enabling continuous operation at higher magnetic field. Naturally, these attributes of HTS are opening new opportunities for applications that benefit from improved magnets (Haught *et al.* 2007; Fietz *et al.* 2013; Whyte *et al.* 2016; Maingi *et al.* 2019). Robust efforts are ongoing to deploy HTS technology towards large-bore high-field magnets for magnetic fusion energy applications (Sorbom *et al.* 2015; Sykes *et al.* 2018).

While worldwide focus has been largely directed towards high-field planar magnet systems, little attention has been paid to new opportunities enabled by HTS technology in applications that benefit from improved non-planar magnets. Non-planar configurations can be found in force-balanced (helical) coils for magnetic energy storage (Miura, Sakota & Shimada 1994), particle accelerator magnets using saddle/bedstead (Thomas, Faircloth & Jago 2005) or canted cosine theta (Amemiya *et al.* 2015) geometries and the stellarator concept of a magnetic fusion energy system (Najmabadi & Raffray 2006; Wolf 2008).

The unusual (essentially two-dimensional) form factor of HTS tape has given rise to several methods to convert such tape into a viable conductor. Integrated multi-tape conductor concepts include: interleaving HTS tapes into a Roebel assembly (Goldacker *et al.* 2007), winding HTS tape helically along a cylindrical form (termed cable on round core conductor (Weiss *et al.* 2017)) and forming stacks of many HTS tape layers and winding the stack in various arrangements (termed twisted stacked-tape conductor (Takayasu *et al.* 2012)). However, the first and still the simplest method to construct a magnet from HTS tape is simply to wind the HTS tape in a 'bare' non-insulated and non-epoxy-impregnated configuration around a bobbin that defines the shape of the final coil. This type of coil is referred to as a non-insulated HTS (NI-HTS) coil (Hahn *et al.* 2011; Kim *et al.* 2012).

1.1. *Primer on benefits and drawbacks of NI-HTS magnets*

A central benefit of the NI-HTS magnet is its simplicity. In this configuration the HTS tape is wound directly onto a shaped bobbin that defines the winding geometry, with the turns usually arranged in a double-pancake geometry. The desired magnet performance (in kiloamp turns, kAt) is then achieved by adding turns to each pancake, or deploying multiple double pancakes. These coils do not require (and indeed cannot allow) cooling channels within the conductor stack. Any heat generated must instead be rejected through the bobbin structure. Also, as the number of turns in the NI-HTS magnet is generally very large, a low supply current is required to drive them in steady state.

Beyond simplicity, owing to the absence of an insulator between turns, NI-HTS magnets offer a degree of intrinsic superconductivity quench protection. This is because the electrical current is offered a multitude of parallel paths to avoid any non-superconducting failure point (Kim *et al.* 2012; Hahn *et al.* 2016) and significant headroom to the critical temperature for superconductivity generally exists. Indeed, NI-HTS quenches are observed to appear as soft limits, as opposed to hard destructive events (Brittles & Bateman 2019). Despite these promising results, the quench dynamics of large-scale NI-HTS coils is still at the frontier of HTS magnet research.

Finally, as the HTS tape itself consists of superconducting layers deposited onto a steel substrate, winding an NI-HTS tape magnet on a steel bobbin results in a final assembly mechanically very similar to pure steel. This yields reduced differential thermal expansion issues and significantly enhanced strength as compared to other magnets.

Drawbacks can also be identified. Owing to the large number of turns of conductor (N) required, NI-HTS coils are typically high in inductance ($L \propto N^2$) and thus cannot quickly change current, with a less inductive path instead followed. These considerations challenge use of NI-HTS coils in alternating current or pulsed operating modes and favour deployment to truly steady-state applications, such as long-time-scale energy storage, particle accelerators and the stellarator fusion concept. Notably, NI-HTS would be challenging to use in the central solenoid and poloidal field coils of the tokamak fusion concept due to the time-varying current requirement, though the toroidal field coils are steady state.

The NI-HTS coil also suffers from a second drawback. For large-bore, high-field applications, the number of turns (and/or the number of double pancakes) required is very large, as is the path length of each turn. Either severely long lengths of HTS tape or a large number of resistive joints are thus required, creating a practical limitation to the ultimate potential of this magnet type. These drawbacks naturally drive large-scale development towards the complex multi-tape conductor assemblies as described earlier.

1.2. Compatibility of NI-HTS magnets with non-planar applications

Considering deployment of NI-HTS magnets to non-planar applications, two additional constraints arise. First, the radius of curvature along the winding trajectory no longer points towards a fixed point, but instead can take arbitrary form. This necessitates the introduction of hard-way bending strain and torsional bending strain. While nearly planar geometries like HTS tape easily tolerate out-of-plane (easy-way) bending (akin to folding paper) they do not tolerate in-plane (hard-way) bending (akin to stretching paper). Second, the magnetic field generated by the magnet is no longer predominantly parallel to the HTS tape plane (as it is in a planar magnet), but instead has significant transverse field components (B_{\perp}). Both of these issues degrade the HTS tape performance and ultimately limit its operating space.

In this work a new winding angle optimization method is developed and presented to mitigate the aforementioned HTS tape compatibility issues of strain and transverse field. The winding angle is a free parameter for any fixed filamentary coil model, and will here be exploited as an optimization parameter to mitigate the issues associated with deploying NI-HTS coils in non-planar applications. Realizing a complex yet mechanically rigid bobbin with tracks at the optimized winding angle is enabled by additive manufacturing. Implicit in using the winding angle to optimize against engineering constraints is the assumption that it has minimal impact on the physics mission (via field errors). This assumption should be valid for the high current densities enabled by HTS technology, but if not additional constraints would be needed in the optimization here discussed. Note that these compatibility issues also generally apply to bending HTS multi-tape cable assemblies (Bykovsky *et al.* 2015). However, in a cable assembly the tape orientation is not available for optimization, unlike in the NI-HTS concept. This offers the opportunity to significantly increase the performance and geometric flexibility of a non-planar NI-HTS magnet as compared to HTS cable assemblies.

1.3. Goal, structure and summary of work

The goal of this paper is to discuss the compatibility of NI-HTS coils for non-planar applications (in particular the mid-scale stellarator), and to present a novel winding angle optimization method developed to overcome the identified limitations. For fixed input non-planar coil filamentary geometry, the winding angle is to first order a free parameter. The optimization method is described in § 2, and the candidate non-planar coil geometries examined (well-known stellarator designs) are described in § 3. Results of strain-only

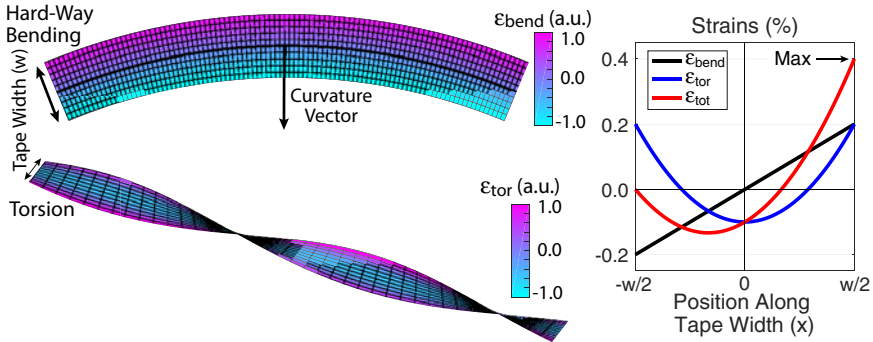


FIGURE 1. Visualization of the strain components considered in the optimization. The hard-way bending strain (ϵ_{bend} , top left) is linearly proportional to the distance along the HTS tape width, while the torsional strain (ϵ_{tor} , bottom left) takes an offset-parabolic form. The peak strain (ϵ_{tot}) is simply found by summing these two components, and it is always found at one edge of the HTS tape.

optimizations are presented in § 4. These optimizations are able to assess the minimum size of a non-planar coil that can be wound without exceeding strain limits for a given width of HTS tape, which are found to be between 0.3 and 0.5 m in mean coil radius for the studied stellarator configurations. Identifying the minimum size allows identification of a mid-scale stellarator capable of achieving high-field or high-temperature operation with minimal HTS tape length. Results of combined strain and B_{\perp} optimizations are presented in § 5. By defining coils larger than the minimum size, headroom is created to allow reduction of the B_{\perp} component, enabling access to higher field for fixed HTS tape length, or the same field at reduced HTS tape length. Alternatively, strain-optimized larger coils permit the use of wider (higher current capacity) HTS tapes. The degree of benefit depends on the target coil size and geometry, as this method can quantify. Conclusions are presented in § 6. The appendix contains a discussion of how to optimize the stellarator coil geometry itself for improved compatibility with NI-HTS magnets, a topic that can open new opportunities in configuration design. As the magnetic fields used to confine stellarator plasmas arise predominantly from external coils, the geometry and specification of these coils define the stability and confinement of the plasma, oftentimes increasing coil complexity to achieve favourable plasma properties (Ku & Boozer 2010).

2. Winding angle optimization method

By calculating the peak strain due to hard-way bending (ϵ_{bend}) along with B_{\perp} along the coil trajectory as a function of winding angle (θ_{wind}), a trajectory can be found that minimizes arbitrary cost functions of these two metrics. To minimize torsional strain (ϵ_{tor}) a tensioned spline fit to the optimal trajectory allows identification of the optimum trade-off between the cost function and ϵ_{tor} . Each of these steps is now described in detail.

2.1. Strain considerations

Two strain components are possibly severe in non-planar coils made with NI-HTS tape, as illustrated in figure 1. These are the hard-way bending strain (ϵ_{bend}) and the torsional strain (ϵ_{tor}) (Takayasu, Minervini & Bromberg 2010).

The hard-way bending strain is linearly proportional to the distance along the HTS tape width, and the magnitude depends on the radius of curvature via the following simple

relationship:

$$\epsilon_{\text{bend}}(x) = \frac{x}{|r_C|}, \quad (2.1)$$

where r_C is the radius of curvature and x is the position along the tape width w . It peaks at $x = w/2$, the tape edge, with a value of $\epsilon_{\text{bend}} = w/2|r_C|$. Here r_C is calculated numerically using finite differences (Wang *et al.* 2017), though if the coil trajectory is parametrized it can also be described analytically using the Frenet–Serret formulas (Gray, Abbena & Salamon 2006).

Note the easy-way bending strain is also given by a similar relation, but it is smaller by the ratio of the tape width to its thickness. As normal HTS tape widths are 4, 6 and 12 mm while thicknesses are 0.1 mm, this strain component can be safely ignored. This also means that as long as the radius of curvature is directed along the major axis of the tape, a 40–120 times smaller radius of curvature can be tolerated. This can greatly impact optimization of the coil trajectory itself as will be discussed separately in the [appendix](#). Note that easy-way strain is ignored in this study because it is so much lower than hard-way strain.

The torsional strain (ϵ_{tor}) does not depend on the local radius of curvature but instead is related to the angular rate of change of r_C along the coil trajectory. The torsional strain takes the form (Takayasu *et al.* 2010)

$$\epsilon_{\text{tor}}(x) = \frac{1}{2} \left(\frac{\Delta\theta_{\text{wind}}}{\Delta L} \right)^2 \left(x^2 - \frac{w^2}{12} \right) \quad (2.2)$$

for a position x along the tape width w , where $\Delta\theta$ is the angular rate of change of the winding angle θ_{wind} per unit length along the coil trajectory (ΔL). Here ϵ_{tor} takes an offset-parabolic form and also peaks at the tape edge ($x = \pm w/2$), with a value of $\epsilon_{\text{tor}} = (\Delta\theta_{\text{wind}}/\Delta L)^2 w^2/12$. Parameter $\Delta\theta_{\text{wind}}$ is also calculated numerically using finite differences, but it too can be described analytically using the Frenet–Serret formulas if the trajectory is parametrized.

A scalar metric representing the total strain ($\equiv \epsilon_{\text{tot}}$) is now defined from ϵ_{bend} and ϵ_{tor} . To rigorously treat the problem, the three-dimensional internal strains at every point in the tape should be taken into account using the principal strain method (Roark, Young & Plunkett 1976), including actual material properties such as the Poisson ratio, modulus of elasticity and modulus of rigidity to relate the different strain tensor elements. To simplify the problem and avoid sensitivity to material properties, a less rigorous but more conservative metric is used in this work – the maximum of a scalar sum of the ϵ_{bend} and ϵ_{tor} components:

$$\epsilon_{\text{tot}} = \max(\epsilon_{\text{bend}}(x) + \epsilon_{\text{tor}}(x)). \quad (2.3)$$

Note that the maximum ϵ_{tot} always occurs at one tape edge or another ($x = \pm w/2$), based on the relative directions of ϵ_{bend} and ϵ_{tor} . This method is conservative because it assumes the strain components are fully collinear (which is approximately true in the limit of thin tapes). Comparison of (2.3) and the principal strain method finds the strain can be overestimated by 15–20 % by (2.3). This overestimate is expected to be compensated by increases in the real material strain introduced by material imperfections, giving additional credence to this conservative approach.

In terms of a limit to the acceptable ϵ_{tot} , in principle empirical data should be gathered at the target operating strain and field conditions to validate the expected performance of the HTS tape. In the absence of such data this study uses an industry rule-of-thumb, which is that a maximum ϵ_{tot} limit of 0.4 % should be enforced (Allen, Chiesa & Takayasu 2015;

Takayasu & Chiesa 2015). Above this limit there is a risk of reduction in the critical superconducting current I_{crit} capacity as well as delamination of the internal layers within the HTS tape (Zhang *et al.* 2016). Regardless, the optimization framework can take arbitrary strain limits as input, and results are generally given in terms of peak predicted ϵ_{tot} .

2.2. Transverse field considerations

Strain is the primary consideration in mid-scale coils as they can easily encounter limits with severe mechanical consequences. Notwithstanding this, the magnitude of the magnetic field transverse to the HTS tape plane (B_{\perp}) is also an important consideration. Large B_{\perp} imposes a soft limit on HTS tape performance as it degrades I_{crit} . Indeed, as progressively larger coils are considered, the most important factor can shift from strain to B_{\perp} , as strain issues are more easily avoided due to large size. Furthermore, larger coils can allow the use of HTS tapes narrower than the maximum allowable width, which would also emphasize B_{\perp} over strain. For this study, data on this limitation are obtained from publicly available HTS tape manufacturer data (Superpower 2018).

Note that unlike the strains, B_{\perp} depends on coils throughout the entire configuration. As such, to compute B_{\perp} the fields from all conductors in the configuration must be taken into account. This includes all other magnets as well as the fields from other turns within the magnet. A limitation of the present study is that a single-filament approximation for each magnet is taken, ignoring the finite coil winding pack size. This approximation will not materially affect B_{\perp} arising from other magnets as long as their separation is large compared to the winding pack size. Since the contribution to B_{\perp} from the other magnets is what can be optimized by changing θ_{wind} , this approximation should also not materially impact the optimization results. The total magnitude of B_{\perp} is, however, underestimated, as this is affected by the winding pack geometry (size and aspect ratio). A second limitation is that additional strain may also arise from the transverse load arising from the HTS tape current crossing B_{\perp} . Quantification of this requires specifying both material properties as well as the target operating field and is outside the scope of the present study. However, this load should be reduced by minimizing B_{\perp} via θ_{wind} optimization. These limitations may be improved upon in the future.

2.3. Optimization philosophy and cost function definition

As the ϵ_{bend} limit is a hard constraint on the HTS integrity, while B_{\perp} is a softer limit, the optimization philosophy is thus to first ensure strain is within tolerable limits, and then within these limits to optimize against B_{\perp} as a secondary constraint. Since ϵ_{bend} and B_{\perp} are single-valued functions of the winding angle θ_{wind} , they can be directly computed for all possible θ_{wind} . In contrast, ϵ_{tor} depends on the gradient of the final θ_{wind} trajectory and is thus not known *a priori*. Calculated ϵ_{bend} and B_{\perp} for all possible θ_{wind} are shown in figure 2(b) for a single point along an example coil trajectory (the coil geometries considered are described in § 3). As can be seen, ϵ_{bend} depends sensitively on the HTS tape width, while B_{\perp} naturally depends on the coil current. As can also be seen, the optimal θ_{wind} to minimize B_{\perp} and ϵ_{bend} are different. Aligning θ_{wind} to the local curvature ensures $\epsilon_{\text{bend}} = 0$, noting that this can be achieved on either the bobbin effective outer diameter or inner diameter.

The method chosen to enable simultaneous optimization of ϵ_{bend} and B_{\perp} is to define a cost function that is a linear sum of ϵ_{bend} and B_{\perp} with an *ad hoc* relative scale factor α .

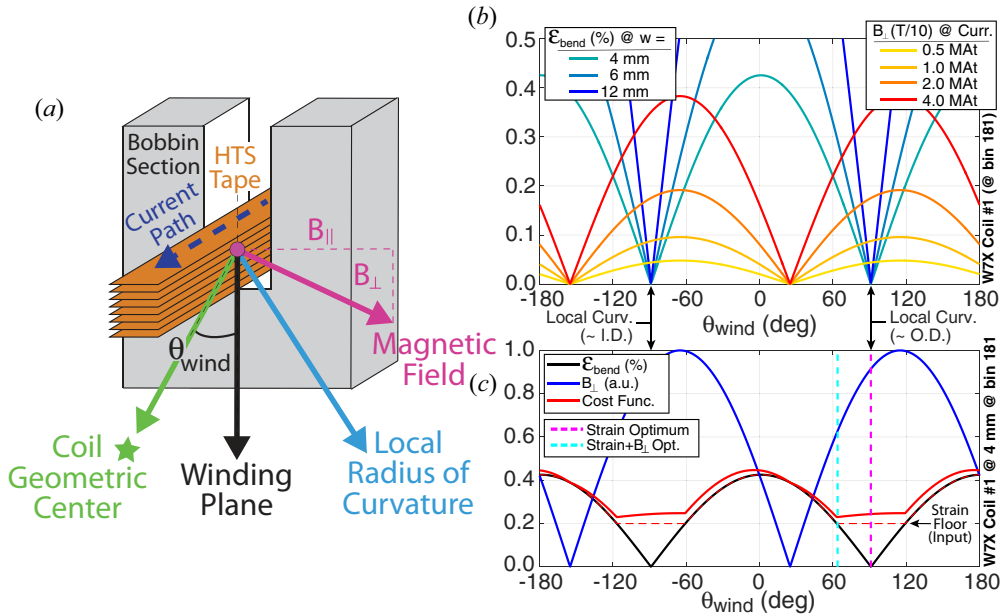


FIGURE 2. (a) Schematic illustration of an NI-HTS coil section and example orientations of the winding angle (θ_{wind}), the magnetic field direction including components parallel ($B_{||}$) and transverse (B_{\perp}) to the HTS tape plane and the local radius of curvature. Note that θ_{wind} is defined relative to the coil geometric centre. For simplicity, only one pancake is shown though several may be defined within a single bobbin, forming multiple double-pancake patterns. (b) Example evaluations of the hard-way bending strain (ϵ_{bend}) and transverse field (B_{\perp}) as a function of θ_{wind} , with minima of each occurring for different θ_{wind} . Strain ϵ_{bend} depends on the HTS tape width while B_{\perp} depends on the coil current. If θ_{wind} is aligned to the local curvature then $\epsilon_{bend} = 0$. (c) Construction of a cost function, (2.4), allowing B_{\perp} to be reduced while maintaining ϵ_{bend} below an input tolerable strain floor ϵ_0 . Solutions exist on both the bobbin effective outer diameter (O.D.) and inner diameter (I.D.).

The cost function is defined as

$$\left. \begin{aligned} \epsilon_{bend} + \alpha B_{\perp} & \text{ if } \epsilon_{bend} > \epsilon_0, \\ \epsilon_0 + \alpha B_{\perp} & \text{ if } \epsilon_{bend} < \epsilon_0. \end{aligned} \right\} \quad (2.4)$$

The parameter ϵ_0 is the bending strain that is deemed to be tolerable and is an input free parameter. An essential feature of the cost function is that when ϵ_{bend} is below ϵ_0 the cost function sees no variation arising from ϵ_{bend} and instead minimizes B_{\perp} . In this way, the cost function can accommodate smaller-size strain-constrained geometries as well as larger-size geometries where strain is less of an issue. Note that ϵ_{tor} is not included in the cost function, since it depends on the gradient of the θ_{wind} trajectory chosen (but not on θ_{wind} itself) and thus cannot be calculated *a priori*. Optimizing for ϵ_{tor} is discussed in the next section. An example cost function as applied to the same coil configuration is shown in figure 2(c). As can be seen, as long as the relative scale factor $\alpha \ll \max(B_{\perp}) / \max(\epsilon_{bend})$, the B_{\perp} term will only have an effect when $\epsilon_{bend} < \epsilon_0$, as desired. If B_{\perp} considerations are ignorable, setting $\alpha = 0$ results in a cost function equal to only ϵ_{bend} .

2.4. Torsion optimization via tensioned splines

Definition of a cost function to optimize θ_{wind} is not sufficient to solve the optimization problem, as the chosen θ_{wind} trajectory itself impacts the total strain via the torsional strain ϵ_{tor} . This is because ϵ_{tor} is related to the rate of change of the chosen θ_{wind} (but not to θ_{wind} itself) along the trajectory. To address this problem, the approach is to compute the cost function (excluding ϵ_{tor}) across all possible θ_{wind} at all positions along the coil trajectory, where it is well defined. This gives rise to contour plots of the cost function that visualizes the optimization problem, and provides a graphical method to reduce ϵ_{tor} while minimally increasing the cost function via the use of tensioned splines.

To simply illustrate this step of the optimization process a ϵ_{bend} -only cost function ($\alpha = 0$ in (2.4)) is used, and only a subset of the coil trajectory is shown in figure 3. As can be seen, the contours in figure 3(a) are simply ϵ_{bend} contours along the coil trajectory for all possible θ_{wind} . The final θ_{wind} is fitted to the minimum of the cost function (the minimum of ϵ_{bend} in figure 3) using a tensioned spline approach. The magnitude of the local radius of curvature is used as a fitting weight for the tensioned spline, with low-curvature regions ascribed a low weight. Additionally, manual adjustment of the fit is possible by inserting points with high weighting to the fitting. This can drive the fit to find alternative optimal paths through the winding trajectory. Different fitted trajectories of θ_{wind} are indicated as the coloured lines in figure 3, with different tensions for each. For low spline tension, the fit closely matches the cost function minimum, while for high tension the variation of θ_{wind} along the coil trajectory is minimized. As can be seen in figure 3(b–d), this allows a direct trade-off between ϵ_{bend} and ϵ_{tor} , and enables a minimum $\epsilon_{\text{tot}} (= \epsilon_{\text{bend}} + \epsilon_{\text{tor}})$ to be identified. Note that in some instances the optimal θ_{wind} trajectory includes regions where winding is primarily on the inner diameter of the coil ($\theta_{\text{wind}} \approx 180^\circ$), as opposed to the outer diameter ($\theta_{\text{wind}} \approx 0^\circ$).

While this method is surely not a unique solution to the optimization problem, the simple treatment is found to be sufficiently flexible to achieve the desired reduction in B_\perp within allowable ϵ_{bend} constraints.

At this point a key difference between this method and the method of calculating space-preserving maps (Gray *et al.* 2006), giving rise to developable surfaces (also called the constant-perimeter method), should be clarified. As a result of the tensioned spline method utilized here, the optimal winding angle θ_{wind} does not necessarily follow the radius of curvature. As such, the final tape surface is not an area-preserving map, and indeed this is why finite ϵ_{bend} is present. Were an area-preserving map method utilized, the resultant trajectory would likely undergo severe ϵ_{tor} as a result of its inability to trade off ϵ_{tor} with ϵ_{bend} , as is done here. Also to be noted is that the optimization workflow also can treat a planar coil, in which case the optimal θ_{wind} returns zero throughout as expected.

3. Stellarator coil configurations considered

Though the optimization methods described in § 2 are applicable to arbitrary coil geometry, well-known yet complex coilsets from the stellarator are used as examples for winding angle optimization with these fixed input filamentary coil geometries. The configurations studied are the Helically Symmetric Experiment (HSX) (Anderson *et al.* 1995), the Wendelstein 7-X (W7-X) stellarator (Beidler *et al.* 1990; Klinger *et al.* 2013) and the National Compact Stellarator Experiment (NCSX) (Zarnstorff *et al.* 2001; Chrzanowski *et al.* 2007). Each coilset was generated primarily based on varying constraints arising from plasma physics, alongside engineering constraints from the coilsets. Note that each configuration differs in physical size and magnet technology (HSX and NCSX are copper while W7-X is LTS). These coils, along with identifying coil

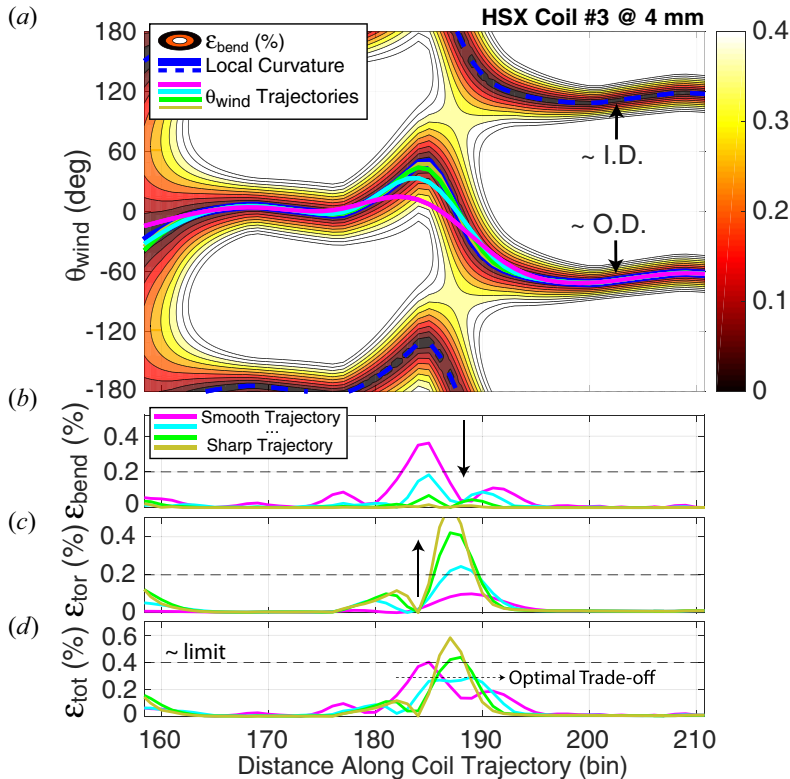


FIGURE 3. Example use of spline tension to minimize total strain. (a) The cost function (here ϵ_{bend}) is plotted for all winding angles (θ_{wind}) for a subset of an example coil trajectory. Varying the spline tension yields various possible θ_{wind} trajectories. (b–d) These different trajectories trade off ϵ_{bend} and ϵ_{tor} differently, giving rise to an optimum in the total strain (ϵ_{tot}).

numbers assigned for the purpose of this study, are shown in figure 4. Note that figure 3 used the no. 3 coil of the HSX configuration.

In order to assess sensitivity to coil size and to estimate the minimum buildable coil size, a uniform geometric scale factor was applied to each of the stellarator configurations shown in figure 4. The average coil radius ($\langle r_{\text{coil}} \rangle$) for each of these designs is plotted against the size scale factor applied in figure 5. Here $\langle r_{\text{coil}} \rangle$ is defined as the mean distance from the filamentary coil trajectory to the coil geometric centre. The coil geometric centre is in turn defined as the mean position of the coil trajectory.

As can be seen, in terms of $\langle r_{\text{coil}} \rangle$, W7-X is the largest though NCSX is only modestly smaller. However, as can be seen in figure 4, the complexity of the NCSX coils is considerably increased due to the more stringent constraints utilized in optimization (in particular the desire for a tight aspect ratio). The HSX coils are smallest and also the most simple. All devices were scaled such that they occupied an overlapping $\langle r_{\text{coil}} \rangle$ range between 0.2 and 0.6 m, with $\langle r_{\text{coil}} \rangle$ used hereafter to parametrize the coil size.

4. Strain optimization and minimum coil size

The main objectives of optimizations involving only strain are to provide headroom to further reduce B_{\perp} and to enable the use of progressively wider HTS tape widths (thus

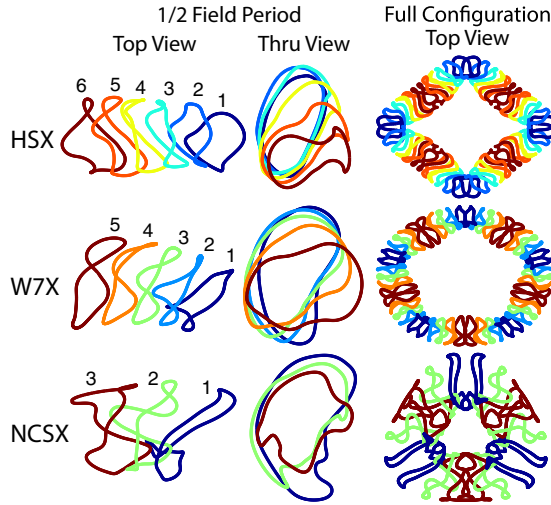


FIGURE 4. Stellarator geometries considered in this study. Non-planar coils in these configurations span from weakly to strongly non-planar.

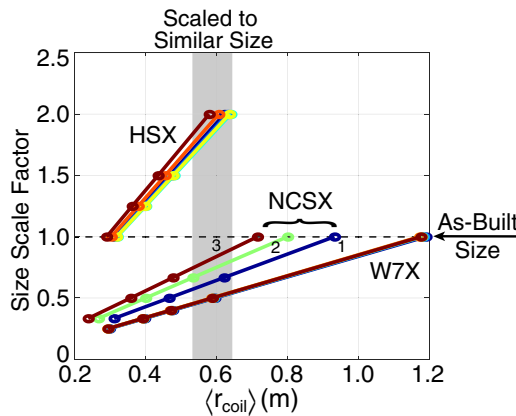


FIGURE 5. Mean coil radius ($\langle r_{coil} \rangle$) for each of the stellarator geometries considered as a function of the size scale factor applied. Size scale factor of 1.0 is the size of the as-built coil.

increasing the current capacity per turn). Strain-only optimizations also provide a means of determining the minimum buildable size of an NI-HTS coil at fixed tape width regardless of target B_{\perp} or alternatively the maximum allowable HTS tape width at fixed size. As described in § 2.1, a value of 0.4% is considered engineering best practice and is here used as the target allowable ϵ_{tot} . Results are conveyed by plotting the peak strain (ϵ_{tot}) versus coil size ($\langle r_{coil} \rangle$), in case further HTS advances modify the allowable strain.

The full coil trajectory for the no. 3 HSX coil shown in figure 4 (and highlighted in figure 3) is shown in figure 6. For this coil, some regions of the coil trajectory are very strongly constrained by ϵ_{bend} while others are not. The tensioned spline approach allows quick identification of the optimal θ_{wind} trajectory.

Figure 7 presents a graphical assessment of the θ_{wind} optimization results and uses the colour axis to highlight the regions where the strain is most severe. As can be seen, the

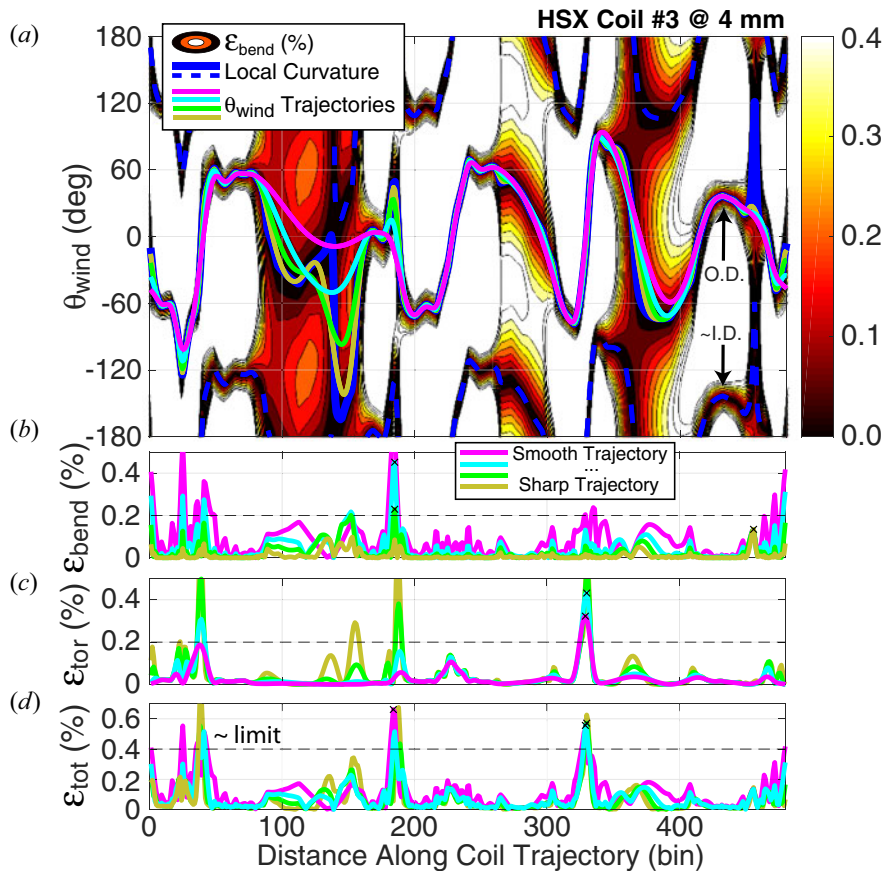


FIGURE 6. The same θ_{wind} trajectories of figure 3 now displayed for the entire HSX no. 3 coil trajectory. Again varying the spline tension yields (a) various candidate θ_{wind} trajectories. (b–d) These different trajectories trade off ϵ_{bend} and ϵ_{tor} differently, giving rise to an optimum in the total strain (ϵ_{tot}).

weak points are in the transition between bends, where some amount of ϵ_{bend} and ϵ_{tor} is unavoidable. Comparing figures 6 and 7, these occur around bins 35, 190 and 330. The winding angle (pink vector in figure 7) changes by a significant amount at these points, yet there is still a finite bend radius.

The impact of size scale factor on ϵ_{bend} , ϵ_{tor} and ϵ_{tot} is shown in figure 8, again using HSX coil no. 3. For each size scale factor, optimization including possible manual intervention as described in § 2.4 has been undertaken. Despite optimization, it is found that the 1.0× size (as-built) coil exceeds the target strain of 0.4%. As such, the as-built HSX is found to be too small to be compatible with the NI-HTS strain limits as here assumed. Increasing the size scale factor naturally reduces the strain, and already by 1.50× scale factor the strain is below the assumed limit.

Using the same methodology, strain assessment as a function of coil size ($\langle r_{coil} \rangle$) was conducted for all coils of the HSX, W7-X and NCSX stellarators. Results are presented in figure 9. As coil size decreases, the target total strain is exceeded, thus defining the minimum buildable $\langle r_{coil} \rangle$ for these existing configurations. Generally, a minimum $\langle r_{coil} \rangle$ of 0.3–0.5 m is found, though variations between coils and configurations exist.

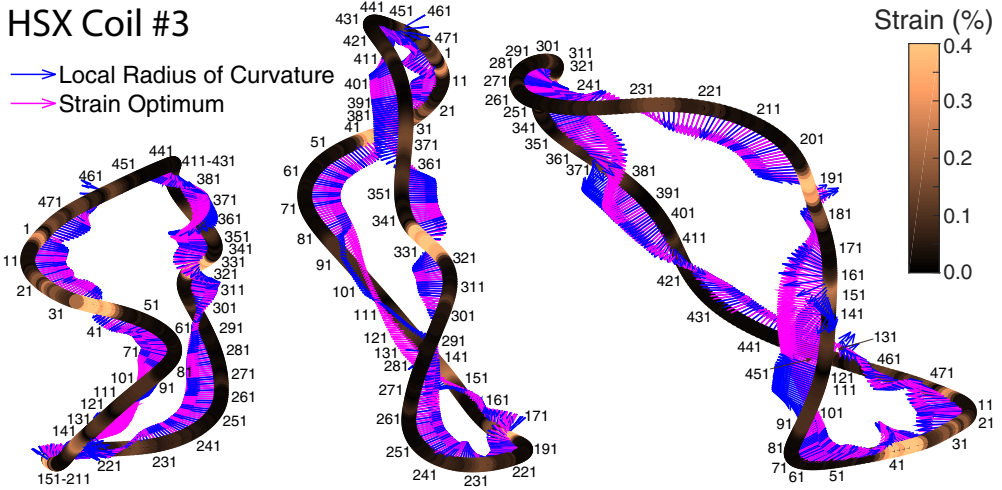


FIGURE 7. Three viewing angles of HSX coil no. 3 showing the local radius of curvature (blue vectors) and optimal θ_{wind} trajectory (magenta vectors) for a strain-only optimization. Colours along the coil trajectory indicate relative ϵ_{tot} . Regions of high ϵ_{tot} are found at the transition between bends.

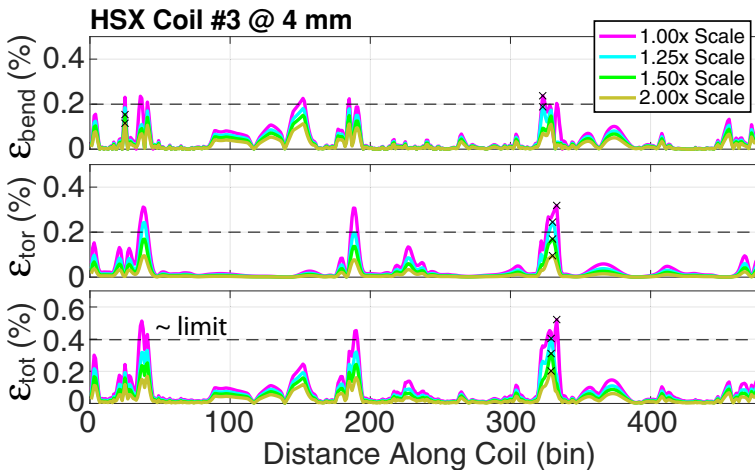


FIGURE 8. Variation of the strain components as a function of size scale factor for HSX coil no. 3. For each size scale factor the trajectory is optimized as in figure 6. The maximum ϵ_{tot} (\times symbols) naturally decreases with size.

Note that HSX coil no. 3 is highlighted because it is most severely limited by strain, despite the fact that it is not the most non-planar. This implies that the degree of non-planar complexity is not directly related to the strain limits encountered, and further suggests optimization of the coil trajectory itself has the potential to significantly improve compatibility with NI-HTS coils. This is further discussed in the [appendix](#).

5. Combined strain and transverse field optimization

Optimizations considering cost functions involving both strain (ϵ_{bend} , defined in § 2.1) and transverse field (B_{\perp} , defined in § 2.2) using cost functions defined in § 2.3 are

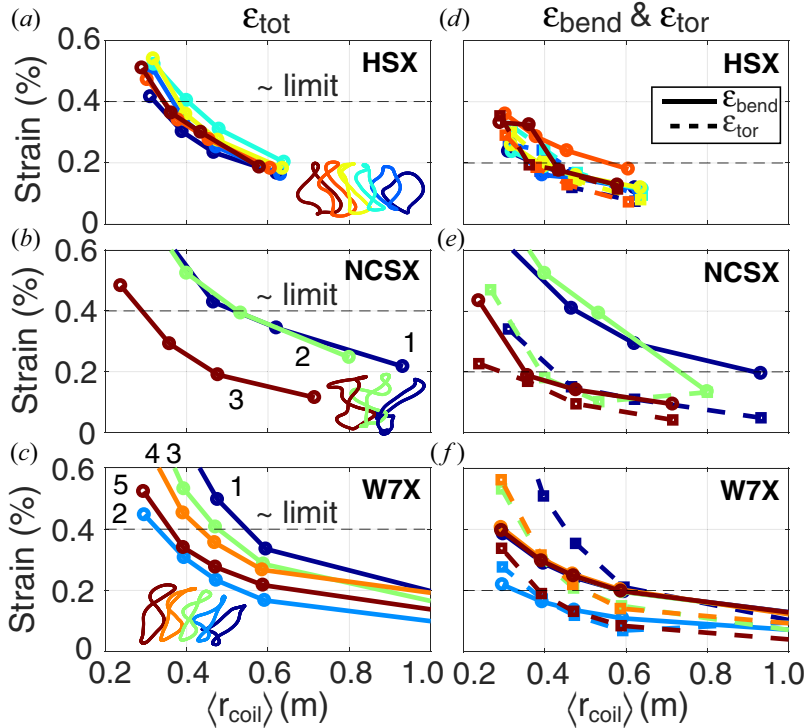


FIGURE 9. (a–c) Peak total strain (ϵ_{tot}) and (d–f) peak bending (ϵ_{bend}) and torsion (ϵ_{tor}) strain for the stellarator configurations as a function of average coil size ($\langle r_{\text{coil}} \rangle$) for 4 mm wide tape. As $\langle r_{\text{coil}} \rangle$ decreases, the target ϵ_{tot} is exceeded, thus defining the minimum $\langle r_{\text{coil}} \rangle$. Each colour indicates a specific coil, with inset coil images as presented in figure 4 included for reference.

now presented. Coils optimized for both considerations must be larger than the minimum coil size ($\langle r_{\text{coil}} \rangle$) shown in figure 9, as headroom in strain is needed to trade off against other factors (like B_{\perp}). As such, B_{\perp} optimization becomes more important as the coil size increases. Furthermore, a design decision needs to be taken that the headroom in strain will be used to mitigate B_{\perp} as opposed to increasing HTS current capacity by increasing the tape width. Recall that to compute B_{\perp} the magnetic fields from all the coils comprising the configuration must be taken into account.

Strain-only (magenta) and combined strain + B_{\perp} (cyan) optimizations are demonstrated for coil no. 1 of the W7-X stellarator configuration, with optimized trajectories shown in figure 10. For this larger coil the larger radii of curvatures yield ϵ_{bend} contours that are significantly lower (figure 10b), enabling deviation of θ_{wind} from the ϵ_{bend} minimum. Contours of B_{\perp} (figure 10c) show a different dependency on θ_{wind} . The combined optimization (cyan lines) follows the cost function target (green) very closely, essentially overlaying. For the combined optimization, ϵ_{tot} now takes a finite value for most of the trajectory (figure 10a), very close to the input ϵ_0 in (2.4) value of 0.2%. The B_{\perp} value was also meaningfully reduced by this method, by nearly 50%.

At this point it should be mentioned that some coils (such as the one highlighted in figure 10) contain apparent artefacts in the coil trajectory that inhibit compatibility with NI-HTS. This can be seen in the wiggles in the local curvature (blue line) in figure 10(b) around bin 210. As size scale factor is reduced, this feature imposes a high strain and

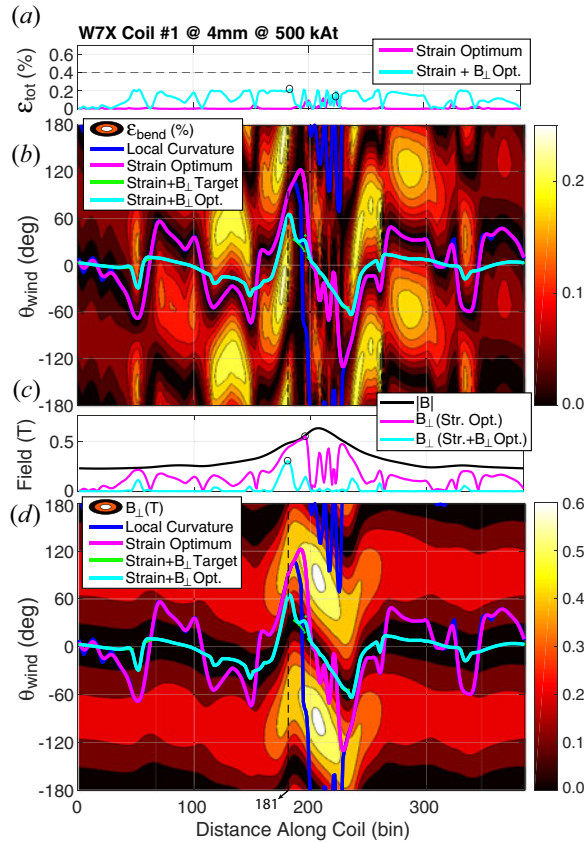


FIGURE 10. Comparison of strain-only (magenta) and combined strain + B_{\perp} (cyan) optimization for W7-X coil no. 1. Evaluations of (a) ϵ_{tot} , (b) ϵ_{bend} versus θ_{wind} , (c) B_{\perp} and (d) B_{\parallel} versus θ_{wind} . Allowing finite ϵ_{tot} enables a significant reduction of B_{\perp} along the optimal θ_{wind} trajectory.

limits the buildable size. As can be seen in figure 11, this artefact occurs at the nominally straight section of the coil. While seemingly straight, these sectors are found to contain finite curvature (and finite ϵ_{bend}) requiring significant torsion (ϵ_{tor}) to mitigate. Improved coil trajectory definition should avoid these artefacts as is described in the appendix.

Using publicly available data on the achievable I_{crit} for a given HTS tape width at various B_{\perp} and operating temperature conditions (Superpower 2018), the HTS tape length needed for a given B_{axis} can be estimated. This is shown in figure 12 for the same trajectories of figure 10 using W7-X coil no. 1. The reduction in B_{\perp} enables a meaningful increase in the achievable B_{axis} for fixed tape width (L_{tape}) or alternatively a reduction in L_{tape} for a fixed B_{axis} .

A second example is provided using the same HSX coil no. 3 described in detail in § 4. However, since the $1\times$ size scale factor was already above the target strain limit, a $2\times$ size scale factor is used. This provides the necessary headroom to, in principle, optimize against both strain and B_{\perp} . However, as shown in figure 13, allowing finite strain does not significantly improve optimization performance, with peak B_{\perp} nearly unchanged. Looking in detail at the constrained region in figure 13(e), ϵ_{bend} is found to be below ϵ_0 only in a

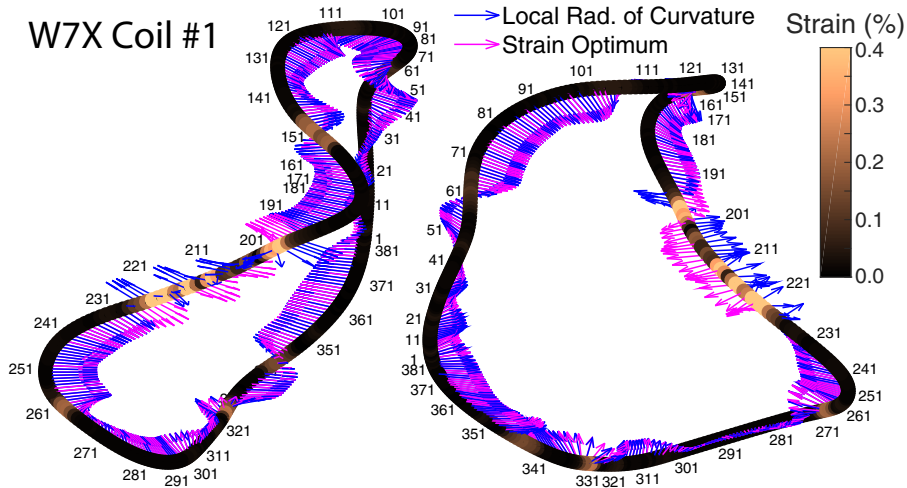


FIGURE 11. Two viewing angles of W7-X coil no. 1 including the local radius of curvature (blue vectors) and optimal θ_{wind} trajectory (magenta vectors) for a strain-only optimization. Colours along the coil trajectory indicate relative ϵ_{tot} . Regions of high ϵ_{tot} are found at the straight section, indicating an artificial constraint is present.

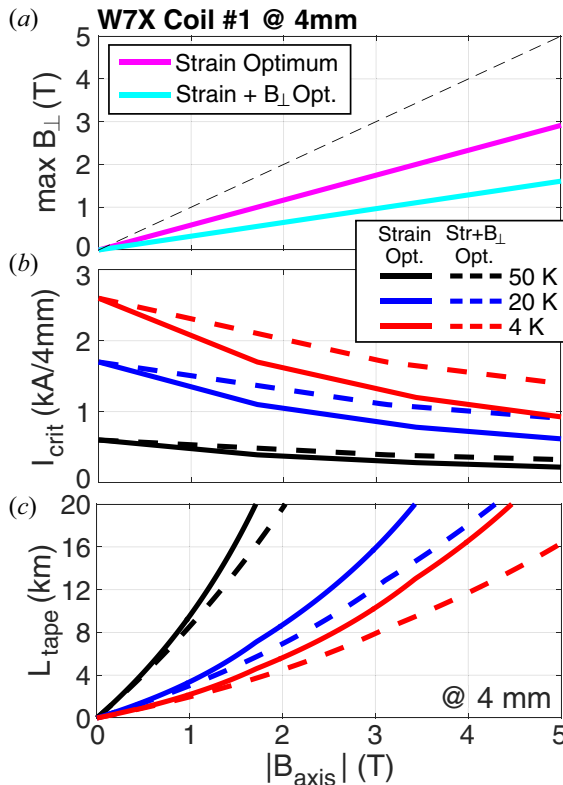


FIGURE 12. (a) Transverse field (B_{\perp}), (b) critical current (I_{crit}) and (c) required HTS tape length as a function of B_{axis} for W7-X coil no. 1.

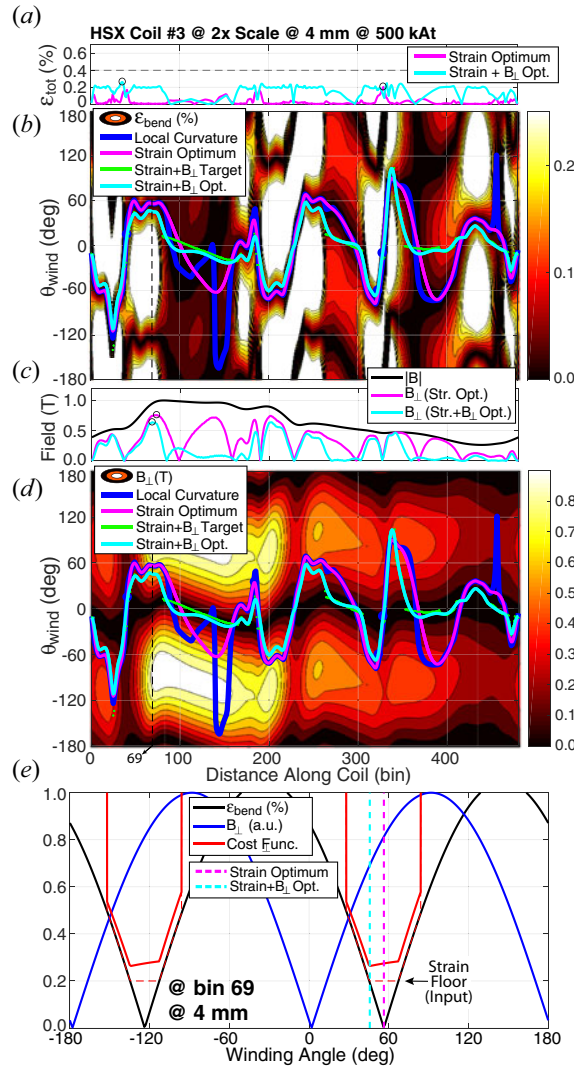


FIGURE 13. Comparison of strain-only (magenta) and combined strain + B_{\perp} (cyan) optimization for HSX coil no. 3 at $2\times$ size scale factor. Evaluations of (a) ϵ_{tot} , (b) ϵ_{bend} versus θ_{wind} , (c) B_{\perp} and (d) B_{\perp} versus θ_{wind} . Allowing finite ϵ_{tot} is not found to improve this optimization by a significant degree, due to (e) a poor alignment of B_{\perp} and ϵ_{bend} constraints around bin 69.

small region of θ_{wind} . Within this allowable θ_{wind} region, no significant B_{\perp} reduction can be achieved. Thus, this particular coil is resistant to further optimization.

Mapping of the I_{crit} data to this coil as B_{axis} is scaled is shown in figure 14 for HSX coil no. 3 at $2\times$ size scale factor. As B_{\perp} did not much change when included in the optimization, both strain only and combined yield similar results. Note that due to the small size, a fairly low L_{tape} is sufficient to access high B_{axis} , revealing a cost-effective path to accessing high- B_{axis} physics at mid-scale enabled by strain optimization.

Combined optimization of all the coils in the HSX configuration at $2\times$ size scale factor is performed and results are given in figure 15. For many coils, the B_{\perp} component could

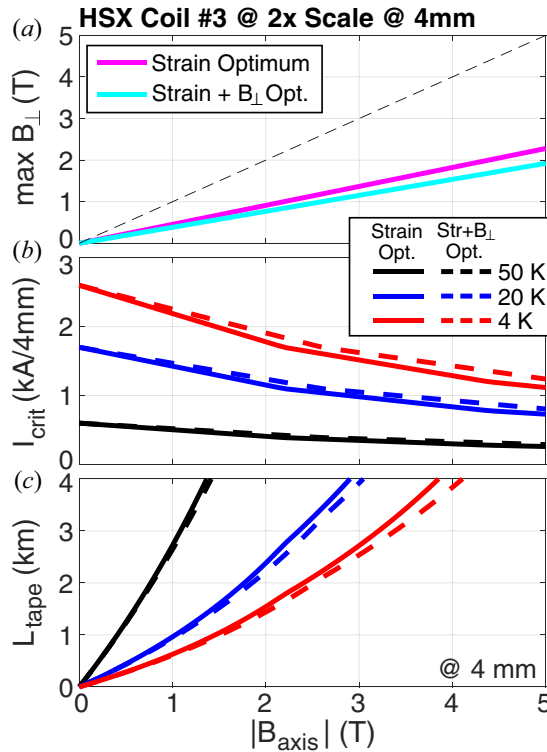


FIGURE 14. (a) Transverse field (B_{\perp}), (b) critical current (I_{crit}) and (c) required HTS tape length as a function of B_{axis} for HSX coil no. 3 at $2\times$ size scale factor. Combined strain + B_{\perp} optimization did not improve the required L_{tape} in this case.

be meaningfully reduced, especially for the least planar coils (nos. 1 and 2). As discussed, coil no. 3 was barely affected, and the other most planar coils less so. Nonetheless, at least in some instances the increased allowance for strain enables a significant reduction in the needed L_{tape} . Final adjudication between all optimization constraints requires a target B_{axis} as well as a notional budget, as increasing L_{tape} implies an increased cost penalty.

6. Discussion and conclusions

This work has presented the benefits and drawbacks of NI-HTS magnet technology specifically for its application to non-planar coils. To first order, for a fixed input non-planar coil filamentary geometry, the winding angle (θ_{wind}) is an unspecified free parameter. A novel winding angle optimization method is here introduced to optimize compatibility with the NI-HTS concept by mitigating the drawbacks of increased hard-way bending strain (ϵ_{bend}), torsional strain (ϵ_{tor}) and increased transverse field (B_{\perp}). By trading off the two strains against each other via an optimized θ_{wind} trajectory, a minimum peak total strain and a reduced B_{\perp} can be obtained. This minimum peak total strain in turn enables assessment of the minimum buildable size for a given input non-planar coil geometry. For well-known existing stellarator designs, the minimum mean coil radius was found to be 0.3–0.5 m for 4 mm wide HTS tape. Identifying the minimum size provides a path to specify a mid-scale stellarator capable of achieving high-field or high-temperature operation with minimal HTS tape length.

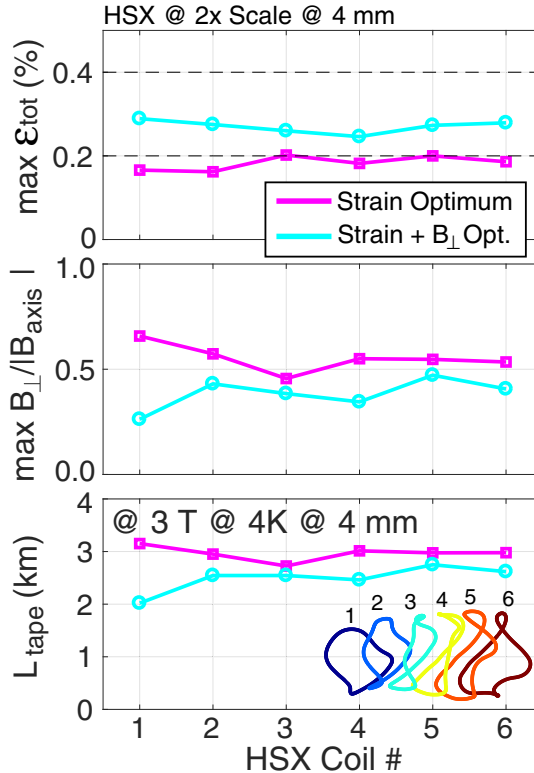


FIGURE 15. Summary of performance improvement via combined strain + B_{\perp} optimization for all HSX coils at $2\times$ size scale factor. The least planar coils (nos. 1 and 2) obtain a meaningful benefit while the more planar coils are fairly constrained and do not benefit as much. In both optimizations, L_{tape} of a few kilometres gives access to B_{axis} of several teslas.

For coils larger than this minimum size, the total strain (ϵ_{tot}) can be traded off against B_{\perp} to reduce this component. This enables a reduction of the length of HTS tape required to achieve a given design magnetic field or equivalently an increase in the achievable magnetic field for constant HTS tape length. Alternatively, optimizing θ_{wind} for a larger size coil would permit the use of wider HTS tapes, thereby increasing the current-carrying capability of each turn and/or winding, thus reducing the number required to achieve the design magnetic field.

Acknowledgements

This work was supported by General Atomics Internal Funds. The author would like to thank A. Benson, B. Breneman, J. Leuer, J. Smith, Z. B. Picc and L. Holland for useful discussions. The author also thanks S. Lazerson and A. Bader for the provision of the existing stellarator device coil geometry information.

Editor Cary Forest thanks the referees for their advice in evaluating this article.

Declaration of interests

The authors report no conflict of interest.

Appendix. Optimization of the coil trajectory for stellarator applications

This work has focused on optimizing the winding angle optimization of a predefined coil to maximize compatibility with NI-HTS magnet technology. Considerations for optimizing the coil trajectory itself now are briefly summarized. This discussion focuses on stellarator applications, as there are many possible degrees of freedom in the coil geometry of these concepts and significant coil optimization work already exists in this area (Merkel 1987; Pomphrey *et al.* 2001; Strickler, Berry & Hirshman 2002; Landreman 2017; Paul *et al.* 2018; Zhu *et al.* 2018a,b).

Stellarator coil optimizations are done with many constraints in mind, most having to do with plasma physics. Considering the constraints arising from the coil technology itself, two constraints are usually included: curvature and coil–coil distance. Interestingly, NI-HTS magnets pose significantly different constraints from those conventionally considered.

First, considering curvature, for an NI-HTS magnet, strain arising from regular curvature is negligible, and is also called ‘easy-way’ bending. The strain issues discussed in § 4 are important, and in particular the interplay of torsion and hard-way bending. If curvature is weakly penalized, yet torsion is not, very different stellarator coil shapes may arise from optimizations against these alternative criteria, particularly with more pronounced toroidal joggles.

Second, considering coil–coil spacing, the compactness (high current density) and mechanical strength (steel substrate and bobbin) inherent to the NI-HTS magnet have the potential to support significantly reduced coil–coil spacing. The final spacing depends on the amount of bobbin material required, which arises from the electromagnetic forces, which require definition of the target operating magnetic field. However, at least as compared to copper and LTS, significantly smaller coil–coil separations can be anticipated.

Finally, stellarator coils are usually parametrized via Fourier series. As for example in the W7-X coil of figure 11, this gives rise to an artefact in the straight sections of the coil where residual undulations exist from incomplete cancellation of the Fourier series. These residual undulations severely compromise compatibility with NI-HTS, despite their origin from a mostly straight section of the coil. Using tensioned splines to parametrize the coil trajectory should remove this artificial limitation.

While outside the scope of this activity, stellarator coil optimizations using these alternative criteria are thus highlighted as fertile ground for future study.

REFERENCES

- ALLEN, N. C., CHIESA, L. & TAKAYASU, M. 2015 Combined tension-torsion effects on 2G REBCO tapes for twisted stacked-tape cabling. *IEEE Trans. Appl. Supercond.* **25** (3), 1–5.
- AMEMIYA, N., MIYAHARA, H., OGITSU, T. & KURUSU, T. 2015 Design of a cosine-theta dipole magnet wound with coated conductors considering their deformation at coil ends during winding process. *Phys. Procedia* **67**, 776–780.
- ANDERSON, F. S. B., ALMAGRI, A. F., ANDERSON, D. T., MATTHEWS, P. G., TALMADGE, J. N. & SHOHET, J. L. 1995 The helically symmetric experiment, (HSX) goals, design and status. *Fusion Sci. Technol.* **27** (3T), 273–277.
- BEIDLER, C., GRIEGER, G., HERRNEGGER, F., HARMeyer, E., KISSLINGER, J., LOTZ, W., MAASSBERG, H., MERKEL, P., NUEHRENBURG, J., RAU, F., *et al.* 1990 Physics and engineering design for Wendelstein VII-X. *Fusion Sci. Technol.* **17** (1), 148–168.
- BRITTLES, G. & BATEMAN, R. 2019 Stability and quench dynamic behaviour of REBCO coils for spherical Tokamaks R&D. In *5th Workshop on Accelerator Magnets in HTS, Budapest, Hungary*, p. Session 2. CERN Indico (indico.cern.ch).

- BRUZZONE, P., FIETZ, W. H. & MINERVINI, J. 2018 High temperature superconductors for fusion magnets. *Nucl. Fusion* **58**, 103001.
- BYKOVSKY, N., UGLIETTI, D., WESCHE, R. & BRUZZONE, P. 2015 Strain management in HTS high current cables. *IEEE Trans. Appl. Supercond.* **25** (3), 4800304.
- CHRZANOWSKI, J., MEIGHAN, T., RAFTOPOULOS, S., FOGARTY, P. J., HEITZENROEDER, P. J., NELSON, B. & WILLIAMSON, D. 2007 NCSX modular coil fabrication. In *Proceedings of Symposium on Fusion Engineering (SOFE), Albuquerque, New Mexico*. IEEE.
- FIETZ, W. H., BARTH, C., DROTZIGER, S., GOLDBACKER, W., HELLER, R., SCHLACHTER, S. I. & WEISS, K. P. 2013 Prospects of high temperature superconductors for fusion magnets and power applications. *Fusion Engng Des.* **88** (6–8), 440–445.
- GOLDBACKER, W., FRANK, A., HELLER, R., SCHLACHTER, S. I., RINGSDORF, B., WEISS, K. P., SCHMIDT, C. & SCHULLER, S. 2007 ROEBEL Assembled Coated Conductors (RACC): preparation, properties and progress. *IEEE Trans. Appl. Supercond.* **17** (2), 3398–3401.
- GRAY, A., ABBENA, E. & SALAMON, S. 2006 *Modern Differential Geometry of Curves and Surfaces with Mathematica*, 3rd edn. Chapman and Hall/CRC.
- HAHN, S., PARK, D. K., BASCUÑÁN, J. & IWASA, Y. 2011 HTS pancake coils without turn-to-turn insulation. *IEEE Trans. Appl. Supercond.* **21** (3), 1592–1595.
- HAHN, S., RADCLIFF, K., KIM, K., KIM, S., HU, X., KIM, K., ABRAIMOV, D. V. & JAROSZYNSKI, J. 2016 ‘Defect-irrelevant’ behavior of a no-insulation pancake coil wound with REBCO tapes containing multiple defects. *Supercond. Sci. Technol.* **29** (10), 105017.
- HAUGHT, D., DALEY, J., BAKKE, P. & MARCHIONINI, B. 2007 Overview of the U.S. Department of Energy (DOE) high-temperature superconductivity program for large-scale applications. *Intl J. Appl. Ceram. Technol.* **4** (3), 197–202.
- KIM, Y. G., HAHN, S., KIM, K. L., KWON, O. J. & LEE, H. 2012 Investigation of HTS racetrack coil without turn-to-turn insulation for superconducting rotating machines. *IEEE Trans. Appl. Supercond.* **22** (3), 5200604.
- KLINGER, T., BAYLARD, C., BEIDLER, C. D., BOSCARY, J., BOSCH, H. S., DINKLAGE, A., HARTMANN, D., HELANDER, P., MASSBERG, H., PEACOCK, A., *et al.* 2013 Towards assembly completion and preparation of experimental campaigns of Wendelstein 7-X in the perspective of a path to a stellarator fusion power plant. *Fusion Engng Des.* **88** (6–8), 461–465.
- KU, L. P. & BOOZER, A. H. 2010 Modular coils and plasma configurations for quasi-axisymmetric stellarators. *Nucl. Fusion* **50** (12), 125005.
- LANDREMAN, M. 2017 An improved current potential method for fast computation of stellarator coil shapes. *Nucl. Fusion* **57** (4), 046003.
- MAINGI, R., LUMSDAINE, A., ALLAIN, J. P., CHACON, L., GOURLAY, S. A., GREENFIELD, C. M., HUGHES, J. W., HUMPHREYS, D. A., IZZO, V., MCLEAN, H., *et al.* 2019 Summary of the FESAC transformative enabling capabilities panel report. *Fusion Sci. Technol.* **75** (3), 167–177.
- MERKEL, P. 1987 Solution of stellarator boundary value problems with external currents. *Nucl. Fusion* **27** (5), 867–871.
- MIURA, Y., SAKOTA, M. & SHIMADA, R. 1994 Force-free coil principle applied to helical winding. *IEEE Trans. Magn.* **30** (4), 2573–2576.
- NAJMABADI, F. & RAFFRAY, A. R. 2006 Recent progress in the ARIES compact stellarator study. *Fusion Engng Des.* **81** (23–24), 2679–2693.
- PAUL, E. J., LANDREMAN, M., BADER, A. & DORLAND, W. 2018 An adjoint method for gradient-based optimization of stellarator coil shapes. *Nucl. Fusion* **58** (7), 076015.
- POMPHELY, N., BERRY, L., BOOZER, A., BROOKS, A., HATCHER, R. E., HIRSHMAN, S. P., KU, L. P., MINER, W. H., MYNICK, H. E., REIERSEN, W., *et al.* 2001 Innovations in compact stellarator coil design. *Nucl. Fusion* **41** (3), 339–347.
- ROARK, R. J., YOUNG, W. C. & PLUNKETT, R. 1976 *Formulas for Stress and Strain*, 8th edn., vol. 43. McGraw-Hill Education.
- SORBOM, B. N., BALL, J., PALMER, T. R., MANGIAROTTI, F. J., SIERCHIO, J. M., BONOLI, P., KASTEN, C., SUTHERLAND, D. A., BARNARD, H. S., HAAKONSEN, C. B., *et al.* 2015 ARC: a compact, high-field, fusion nuclear science facility and demonstration power plant with demountable magnets. *Fusion Engng Des.* **100**, 378–405. [arXiv:1409.3540](https://arxiv.org/abs/1409.3540).

- STRICKLER, D. J., BERRY, L. A. & HIRSHMAN, S. P. 2002 Designing coils for compact stellarators. *Fusion Sci. Technol.* **41** (2), 107–115.
- SUPERPOWER 2018 SuperPower Technical Documents. Available at: <http://www.superpower-inc.com/content/technical-documents>.
- SYKES, A., COSTLEY, A. E., WINDSOR, C. G., ASUNTA, O., BRITTLES, G., BUXTON, P., CHUYANOV, V., CONNOR, J. W., GRYAZNEVICH, M. P., HUANG, B., *et al.* 2018 Compact fusion energy based on the spherical tokamak. *Nucl. Fusion* **58** (1), 016039.
- TAKAYASU, M. & CHIESA, L. 2015 Analytical investigation in bending characteristic of twisted stacked-tape cable conductor. *IOP Conf. Ser.: Mater. Sci. Engng* **102**, 012023.
- TAKAYASU, M., CHIESA, L., BROMBERG, L. & MINERVINI, J. 2012 HTS twisted stacked-tape cable conductor. *Supercond. Sci. Technol.* **25** (1), 014011.
- TAKAYASU, M., MINERVINI, J. & BROMBERG, L. 2010 Torsion strain effects on critical current of HTS superconducting tapes. *AIP Conf. Proc.* **1219** (1), 337–344.
- THOMAS, C. M., FAIRCLOTH, D. C. & JAGO, S. J. S. 2005 Magnet design for the ISIS second target station proton beam line. *Proc. IEEE Part. Accel. Conf.* **2005**, 1652–1654.
- WANG, X., ARBELAEZ, D., CASPI, S., PRESTEMON, S. O., SABBI, G. L. & SHEN, T. 2017 Strain distribution in REBCO-coated conductors bent with the constant-perimeter geometry. *IEEE Trans. Appl. Supercond.* **27** (8), 6604010.
- WEISS, J. D., MULDER, T., TEN KATE, H. J. & VAN DER LAAN, D. C. 2017 Introduction of CORC⁶ wires: highly flexible, round high-temperature superconducting wires for magnet and power transmission applications. *Supercond. Sci. Technol.* **30** (1), 014002.
- WHYTE, D. G., MINERVINI, J., LABOMBARD, B., MARMAR, E., BROMBERG, L. & GREENWALD, M. 2016 Smaller & sooner: exploiting high magnetic fields from new superconductors for a more attractive fusion energy development path. *J. Fusion Energy* **35** (1), 41–53.
- WOLF, R. C. 2008 A stellarator reactor based on the optimization criteria of Wendelstein 7-X. *Fusion Engng Des.* **83** (7–9), 990–996.
- ZARNSTORFF, M. C., BERRY, L. A., BROOKS, A., FREDRICKSON, E. D., FU, G.-Y., HIRSHMAN, S. P., HUDSON, S. R., KU, L. P., LAZARUS, E. A., MIKKELSEN, D., *et al.* 2001 Physics of the compact advanced stellarator NCSX. *Plasma Phys. Control. Fusion* **43**, A237.
- ZHANG, Y., HAZELTON, D. W., KELLEY, R., KASAHARA, M., NAKASAKI, R., SAKAMOTO, H. & POLYANSKII, A. 2016 Stress-strain relationship, critical strain (stress) and irreversible strain (stress) of IBAD-MOCVD-based 2G HTS wires under uniaxial tension. *IEEE Trans. Appl. Supercond.* **26** (4), 8400406.
- ZHU, C., HUDSON, S. R., SONG, Y. & WAN, Y. 2018a Designing stellarator coils by a modified Newton method using FOCUS. *Plasma Phys. Control. Fusion* **60** (6), 065008.
- ZHU, C., HUDSON, S. R., SONG, Y. & WAN, Y. 2018b New method to design stellarator coils without the winding surface. *Nucl. Fusion* **58** (1), 016008.